Decadal variability of extreme high temperature in mid- and high-latitude Asia and its associated North Atlantic air–sea interaction

Tao Wang[1,2] · Shuyue Yin[3] · Wei Hua[4] · Huijun Wang[1,2] · Feifei Luo[4] · Jiapeng Miao[1] · Yuanhai Fu[1]

Abstract

The decadal variability of extreme high temperature (EHT) in the mid and highlatitudes of continental Asia (MHLCA) and associated mechanisms were investigated. Observational analysis indicated that, after removing global warming, the first leading mode of the EHT events showed a meridional dipole pattern and had significant decadal variability. During the periods 1980–1994 and 2012–2019 (1995–2011), EHT events were more frequent and stronger (less frequent and weaker) in western-central Siberia than normal, whereas they were less frequent and weaker (more frequent and stronger) in the wide area to the south of Lake Baikal. Further Observational and CESM (Community Earth System Model) results based analysis suggested that decadal change in air–sea interaction in the North Atlantic play an important role in shaping the decadal variability of EHT events in MHLCA. On decadal timescales, meridional negative–positive–negative sea surface temperature (SST) anomalies in the North Atlantic and their coupled positive North Atlantic Oscillation can trigger stronger wave activity flux and cause a significant anticyclonic–cyclonic teleconnection wave train in the troposphere over the mid and high latitudes of the Eurasian continent. As a result, an anomalous high-pressure center is evident in western-central Siberia, and thereby reducing total cloud cover and causing stronger solar heating. Thus, EHT events become more frequent and stronger. On the contrary, for the areas south of Lake Baikal, EHT events are weakened by corresponding cyclonic circulation anomalies. Additionally, the CAM5 (Community Atmosphere Model version 5) experiments suggested more important driving role of the decadal North Atlantic tripole SST anomalies in the abovementioned processes.

Keywords Extreme high temperature · Decadal variability · North Atlantic tripole SST · Middle and high latitudes of continental Asia · Numerical simulation

1 Introduction

In the past 100 years, the global surface temperature has increased by nearly 1 °C, as reported by the intergovernmental panel on climate change fifth assessment report (IPCC 2013). Particularly, from the middle of the 20th century to the present day, global warming has been accelerating (Xu et al. 2018; Cheng et al. 2019), and with it has come more extreme events such as extreme high temperature (EHT) events, extreme heavy precipitation, and exceptionally strong tropical cyclones, occurring in many parts of the world (Rahmstorf and Coumou 2011; Coumou and Rahmstorf 2012; Donat et al. 2013). More seriously, since the beginning of this century, record-breaking monthly mean temperatures have increased worldwide (Coumou et al. 2013). At the same time, record-breaking heat waves struck Europe in 2003 (Schär et al. 2004), Greece in 2007 (Founda and

✉ Tao Wang
wangtao@mail.iap.ac.cn

1 Climate Change Research Center, Institute of Atmospheric Physics, Chinese Academy of Sciences, Beijing 100029, China

2 Collaborative Innovation Center on Forecast and Evaluation of Meteorological Disasters (CIC-FEMD), Nanjing University of Information Science and Technology, Nanjing 210044, China

3 Chengdu Weather Modification Center, Chengdu Meteorological Bureau, Chengdu 611130, China

4 China Joint Laboratory for Climate and Environmental Change, Chengdu University of Information Technology, Chengdu 610225, China

Giannakopoulos 2009), Russia in 2010 (Barriopedro et al. 2011), eastern China in 2013 (CMA 2014), southern China in 2018 (Deng et al. 2020), and Europe again in 2019 (Xu et al. 2020), to name just the main examples. These EHT events caused major damage to ecosystems and society. Taking the 2003 European heat wave as an example, it culminated in 14,800 heat-related deaths in France alone, and also caused heavy casualties in other European centuries such as Italy, Spain, Portugal and the United Kingdom (Bouchama 2004). In the recent 2013 China heat wave, reported heat-related illnesses exceeded 5700 (Gu et al. 2016). Therefore, issues related to EHT have received widespread attention.

Numerous studies suggest that anthropogenic global warming is one of the most important factors resulting in higher frequency and more severe EHT on the global scale (Griffiths et al. 2005; Christidis et al. 2011; Morak et al. 2013; Dong et al. 2016; Kim et al. 2016; Dong et al. 2017). At regional scales, "detection and attribution" studies also indicate the important role played by human activities in increasing the frequency and severity of EHT events (Zwiers et al. 2011; Christidis and Stott 2016; Yin et al. 2017; Chen and Dong 2019; Seong et al. 2021). In the future, in a world that has warmed by 1.5 °C, 2.0 °C or more, human activities will cause more higher-intensity EHT events on both global and regional scales (Chen and Sun 2015; Fischer and Knutti 2015).

In fact, regional EHT events are the result of the combination of natural internal variability of the climate system and anthropogenic emissions of greenhouse gases (Schär et al. 2004; Meehl et al. 2007; Shiogama et al. 2014; Zhou et al. 2014; Sun et al. 2016). Along with mean warming, enhanced variability can also result in more frequent and intense EHT events, and even record-breaking heatwaves (Barriopedro et al. 2011). Thus, natural internal variability also plays an important role in causing regional EHT events (e.g., Wang et al. 2013; Diao et al. 2018).

Horton et al. (2015) suggested that both dynamic and thermodynamic effects can contribute to observed changes in temperature extremes. At most locations, warm extremes are associated with positive 500-hPa geopotential height and sea level pressure anomalies slightly downstream and negative anomalies farther upstream (Loikith and Broccoli 2012; Xu et al. 2019b). EHT events are often accompanied by specific atmospheric circulation patterns, less precipitation, and nearby prolonged hot surface conditions (e.g., Fischer et al. 2007; Lau and Nath 2012, 2014). In inland area, anomalous circulations can advect hot and dry air, and thereby causing the regional EHT events. An anomalous high-pressure center and anticyclone near the surface can also lead to clear sky and thereby greater solar heating, which together are believed to be the main physical driver of hot extremes (e.g., Meehl and Tebaldi 2004; Tomczyk and Bednorz 2016; Cowan et al. 2017; Luo and

Lau 2017; Adams et al. 2021). In addition, the descending branch within the column of the anomalous anticyclone can enhance local adiabatic heating, which also contributes to localized EHT events (Li et al. 2021). Within these processes, soil moisture–temperature feedback is usually involved (Stefanon et al. 2014).

Anomalous sea surface temperature (SST) is one root cause that can lead to large-scale circulation anomalies or local anticyclonic conditions, and ultimately to EHT events. Based on observational and modeling results, Arblaster and Alexander (2012) suggested that extreme maximum temperatures are significantly cooler over Australia, southern Asia, Canada and South Africa during strong La Niña events, as compared to El Niño events, and significantly warmer over the contiguous United States and southern South America. Additionally, tropical Pacific and Indian Ocean warm SST anomalies can influence EHT events over the southern part of China (Hu et al. 2013; Wang et al. 2014; Deng et al. 2019). Even decadal SST anomalies, such as the Pacific Decadal Oscillation and Atlantic Multidecadal Oscillation, have been shown to be closely related to EHT events—specifically, in North China (e.g., Zhang et al. 2020a; Zhu et al. 2020; Yang et al. 2021).

During the period of accelerated global warming in the past few decades, the Arctic region has shown the most significant warming owing to the so-called Arctic amplification effect (Screen and Simmonds 2010). In fact, the mid and high latitudes of continental Asia (hereafter abbreviated to MHLCA), which is adjacent to the Arctic, also show a stronger warming rate compared to other regions Fig. 1 in Xie et al. (2015); and logically, such marked increases in mean surface air temperature (SAT) must lead to similarly large increases in the frequency and severity of EHT events. Moreover, under the future warming scenarios we can expect with unchecked or insufficiently constrained global warming, these increases in the frequency and severity of EHTs event will cause greater impacts on local ecosystems and human society (IPCC 2021). In such a region with the most significant future warming, will natural variability also have an impact on EHT events and superimpose on warming to cause more severe extreme events? To better understand the likely future changes in EHT events in MHLCA, it is particularly important to clarify the mechanism of EHT variation in this area during recent decades. In this study, we will remove the influence of global warming and explore the internal variability factors affecting the decadal variations of extreme high temperature in this region based on 40-year daily observation data and our numerical simulation data.

The rest of this paper is organized as follows: The data, numerical model and methods used in this study are described in Sect. 2. In Sect. 3, the observed spatiotemporal characteristics of EHT in MHLCA, as well as the observed

and simulated mechanisms, are investigated. Conclusions are presented and discussed in Sect. 4.

2 Data, numerical model and methods

The daily maximum temperature (Tmax) from the Climate Prediction Center (CPC) global temperature data provided by the National Oceanic and Atmospheric Administration/ Oceanic and Atmospheric Research/Earth System Research Laboratories Physical Sciences Laboratory (https://psl.noaa. gov/data/gridded/data.cpc.globaltemp.html) was used to calculate the intensity and frequency of EHT for the period 1980–2019. The monthly SAT, which was calculated based on the CPC global temperature data, was used to examine changes in mean SAT in boreal summer (June, July, and August). The observed SST from the hadley center monthly sea surface temperature dataset (Rayner et al. 2003), monthly precipitation in the Climate Research Unit (CRU) data set (Harris et al. 2020), and monthly ERA-Interim data from the European Centre for Medium-Range Weather Forecasts (Dee et al. 2011) are used to investigate related climate change during the period 1980–2019.

The Community Earth System Model (CESM) version 1.2.2, which was developed and is maintained by the National Center for Atmospheric Research, was used to carry out a long-term simulation. This model is a coupled global climate model. It has seven components, including atmosphere, ocean, land, sea ice, land ice, river runoff, and ocean waves. They are coupled by a coupler that coordinates these components' temporal evolution and passes information between them (more detailed information can be found at https://www.cesm.ucar.edu/). A long-term simulation was performed with the "B1850C5" configuration, which means that the external forcing agents had no year-to-year variations. The values for greenhouse gas concentrations, aerosols, and ozone were determined based on the settings from pre-industrial control simulations in Phase 6 of the CMIP (coupled model intercomparison project), and were fixed at preindustrial levels (1850). The horizontal resolution was set to "f19_g16", which means that the horizontal resolutions of the atmosphere and ocean components were approximately 2° (1.9° in latitude and 2.5° in longitude) and 1°, respectively. The initial states used in the experiment were obtained from the b40_1850_c02c_76jpf files, which contain the initial fields for the pre-industrial simulation provided by the National Center for Atmospheric Research (NCAR) through long-term simulations. In this study, we further continuously integrated the 200 model years. The first 100 model years were used as spin-up to allow the model to reach an equilibrium state, accounting for changes in the computing environment and subtle parameters. We analyzed the final 100 years. Analysis of this long-term

simulation can avoid influences from external forcings on the related mechanism and processes. In addition, two simulations using the Community Atmosphere Model version 5 (CAM5), which is the atmospheric component of the CESM, were performed to examine the influence of anomalous SST on EHT in MHLCA. More detailed information can be found in the following simulation result section.

In this study, the EHT intensity was defined as the maximum value of daily maximum temperature in summer of that year. Besides, the EHT frequency was defined as the number of days when the daily maximum temperature in summer of that year was greater than the 90th percentile value in the base period (1981–2010). The 90th percentile value was calculated using the same method as in Bonsal et al. (2001). Take one grid for example, there were 2760 Tmax values (30 years × 92 days in each summer), and they were first sorted in ascending order: $X_1, X_2,…,X_{2760}$. The probability P that a random value is less than or equal to the rank of that value X_m is estimated by $P = (m − 0.31)/(N + 0.38)$. $N = 2760$ and the Tmax representing the 90th percentile was linearly interpolated between the 2484th-ranked value (corresponding to $P = 89.98\%$) and 2485th-ranked value (corresponding to $P = 90.01\%$). In this study, to remove the effects of global warming on the EHT over MHLCA, we detrended the EHT intensity, the EHT frequency and associated observed meteorological variables before analysis. Referring to Zhang et al. (2018), the linear trends were removed for all the observational data to reduce the anthropogenic and other external forcings' influences. For statistical analysis, we mainly used the empirical orthogonal function (EOF) analysis, regression analysis and composite analysis, and the statistical significance of the composite analysis was assessed by applying the Student's t test.

3 Results

3.1 Observed decadal changes in EHT

First, we made an EOF analysis of the detrended anomalies in the frequency and intensity of EHT events during the period 1980–2019. As shown in Fig. 1a and c, the first leading modes of the frequency and intensity of EHT were almost the same, showing meridional dipole modes. These two first leading modes can explain 17.4% and 14.8% of their total variances. Their positive and negative centers were located in western Siberia and the wide area to the south of Lake Baikal, respectively. It suggested that EHT experienced opposite trends in these two areas during the period 1980–2019. Their principal components (PCs) were also consistent during this period (Fig. 1b and d). On the decadal timescale, the two PCs both turned into a negative phase around 1995 and rebounded into a positive phase in
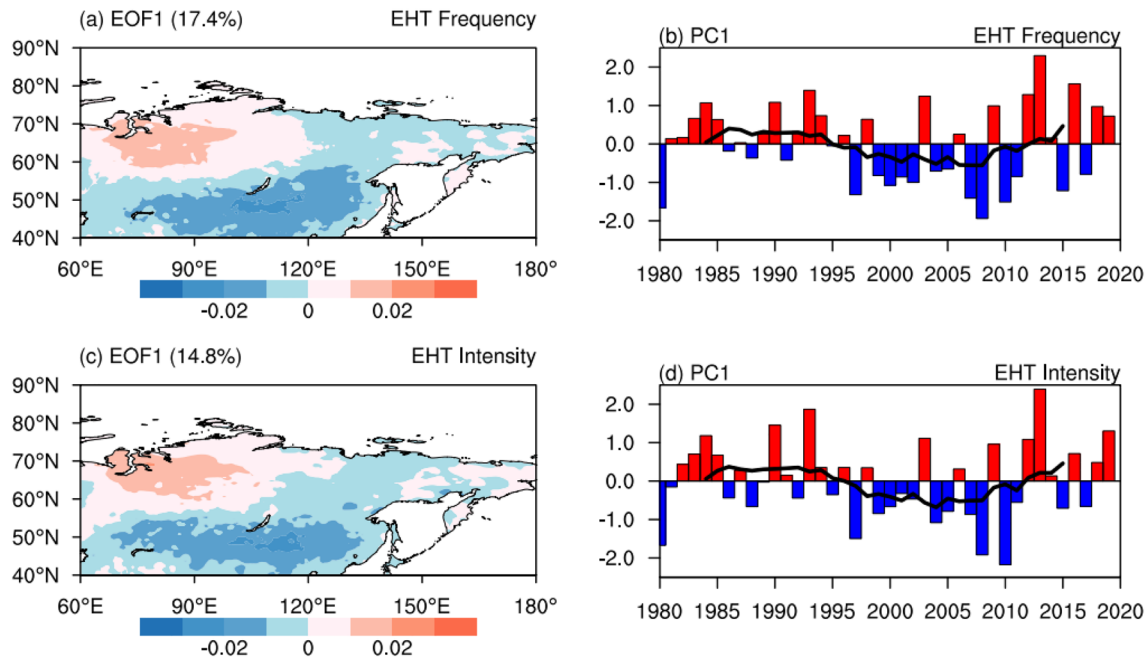
Fig. 1 **a** First leading EOF mode of anomalous summer EHT frequency (unit: days). **b** Normalized PC time series corresponding to the EOF mode of summer EHT frequency during 1980–2019 (bars) and its nine-year running mean (black line). **c**, **d** As in **a**, **b** but for summer EHT intensity (unit: °C)

2012. This indicated that the EHT in MHLCA presented significant decadal variabilities.

The result of a seven-year moving t test further confirmed the decadal shift of EHT and the abovementioned jump points (i.e., the years 1995 and 2012, Fig. 2a). Accordingly, we chose the years from 1980 to 1994 and from 2012 to 2019 as the positive phases and the years from 1995 to 2011 as the negative phase. The composite results were consistent with the above EOF analysis. In western Siberia, the intensity of EHT was stronger and its occurrence was more frequent during the positive phases, whereas EHT was weaker and less frequent during the negative phase (Fig. 2b and c). On the contrary, the EHT in the mid-latitude region south of Lake Baikal showed opposite variations. In the following sections, we explored the mechanisms underpinning the decadal variabilities of EHT during the past 40 years.

3.2 Anomalous atmospheric circulation and North Atlantic SST

Regional atmospheric circulation was very different between the positive and negative phases. As shown in Fig. 3a, anomalous downward vertical motion can be found over western-central Siberia during the positive phases, whereas anomalous upward vertical motion was mainly present south of Lake Baikal and in some eastern Siberian areas. Correspondingly, significant anticyclonic and cyclonic circulation anomalies were evident in these two regions, respectively

(Fig. 3b). Particularly at north of Lake Baikal, sea level pressure anomalies were increased, indicating significant anticyclonic conditions there (Fig. 3c). Due to anomalous vertical motion over MHLCA, the total cloud cover was significantly reduced over western-central Siberia (Fig. 3d). As a result, surface net shortwave radiation was increased in western-central Siberia, and dominanted regional surface heat fluxes (Fig. 4a). Finally, the SAT increased significantly in western-central Siberia (Fig. 3e). In the clear-sky, surface net shortwave radiation didn't show significant changes (Fig. 4b). It suggested that reduced total cloud cover and associated changes in solar radiation were key factors leading to local warming. For some areas south of Lake Baikal, the processes were opposite. Therefore, the anomalous spatial patterns in local circulation and related radiation were consistent with changes in SAT and the decadal variability of EHT events (Fig. 2b, c). This suggested that local circulation anomalies between positive and negative phases was the main reason behind the decadal variability of EHT events in MHLCA.

On a larger scale, a significant anticyclonic–cyclonic teleconnection wave train in the troposphere can be seen in the mid and high latitudes of the Northern Hemisphere (Fig. 5). Over the Eurasia, the anomalous wave train is similar with the British-Baikal Corridor (Xu et al. 2019a), and the local circulation anomalies in MHLCA was one part of this teleconnection wave train. Analysis of the wave activity flux (WAF) suggested that this tropospheric teleconnection wave
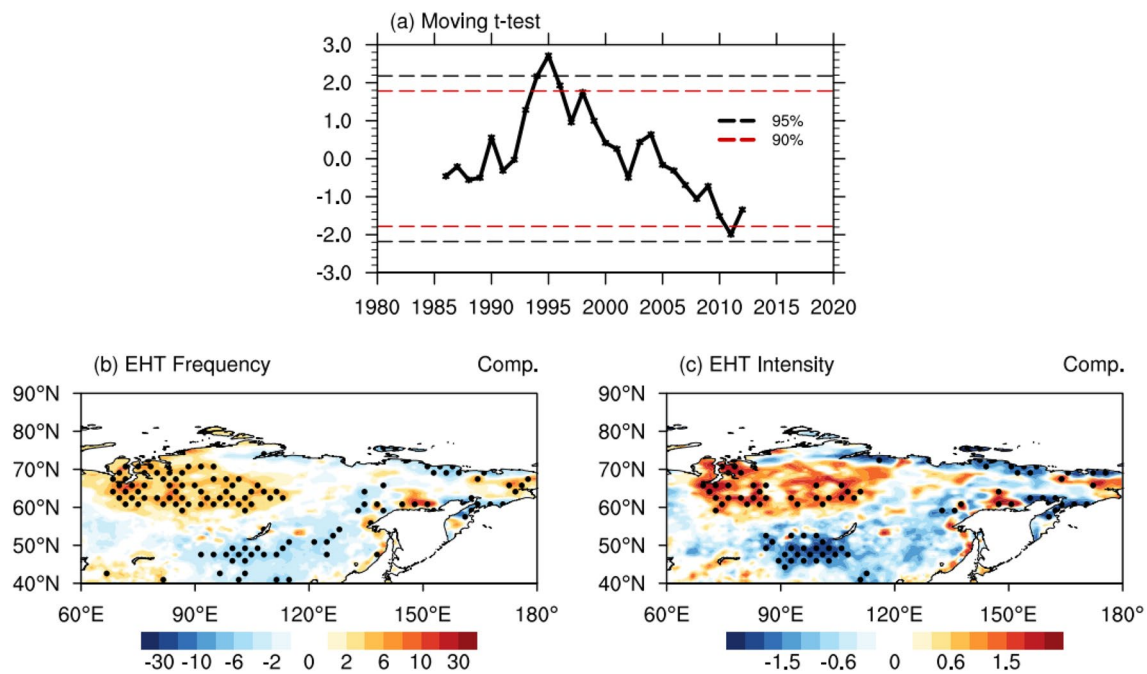
Fig. 2 **a** The moving *t*-test values with two subseries (each duration is 7 years) of the PC1 of the EHT frequency during 1980–2019 (dashed lines represent the 90% and 95% significance level). **b** Differences in the summer EHT frequency (unit: days) between positive (1980–1994 and 2012–2019) and negative phases (1995–2011). **c** As in **b** but for summer EHT intensity (unit: °C). In **b** and **c**, areas that exceed the 95% confidence level are dotted

train probably propagated from the North Atlantic to the high-latitude Asian region. And in the source area of the wave train, positive North Atlantic Oscillation (NAO) was evident (Fig. 5a and b).

Therefore, we further examined the changes in North Atlantic SST between the positive and negative phases. As shown in Fig. 6, during the positive phases, the North Atlantic showed a meridional tripole SST anomaly pattern. Significant negative SST anomalies were evident in the tropics and north of 45ºN in the Atlantic, whereas positive SST anomalies lied between in the mid-latitude Atlantic. Such tripole SST pattern was well coupled with overlying positive NAO-like circulation.

Many previous studies have examined the decadal and longer scale North Atlantic SST variations and their role in modulating climate variabilities over the North Atlantic and Eurasian continent (e.g., Kushnir 1994; Schlesinger and Ramankutty 1994; Sutton et al. 2003; Lu et al. 2020). Actually, the tripole anomaly pattern was a dominant mode of North Atlantic SST variabilities after removing the linear trend. As shown in Fig. 7, this first leading mode can explain 28.2% of the total variance. Including annual variabilities, its PC showed that this tripole SST pattern had significant decadal variations during the past 40 years. This shifting also occurred in the years 1995 and 2012, which were the same years as for the decadal changes in EHT in MHLCA, suggesting there was a close relationship between them.

Such decadal North Atlantic SST pattern and anomalous NAO-like pattern were likely to be the root cause of the wave train in the troposphere, and thereby the decadal changes in EHT in MHLCA.

3.3 Observed remote influences of North Atlantic SST

To highlight the influences of the meridional tripole SST anomalies on the downstream climate, we used a summer North Atlantic tripole index (NATI) in the following analysis. The NATI was defined as (Fig. 7)

$$NATI = normalized\left(SSTA_2 - \frac{SSTA_1 + SSTA_3}{2}\right)$$

These three NATI regions were chosen according to the leading mode (Fig. 7) and decadal change in the North Atlantic SST pattern (Fig. 6). The interannual and decadal variabilities of NATI were consistent with the PC of first leading mode of North Atlantic SST anomalies. The correlation coefficient between them was 0.74 ($p < 0.01$).

Figure 8a and b showed the wind fields at 300 hPa and 500 hPa regressed upon NATI. An anticyclone–cyclone–anticyclone–cyclone–anticyclone pattern was evident in the troposphere from the North Atlantic to central Siberia. This circulation pattern showed a significant wave-train feature,
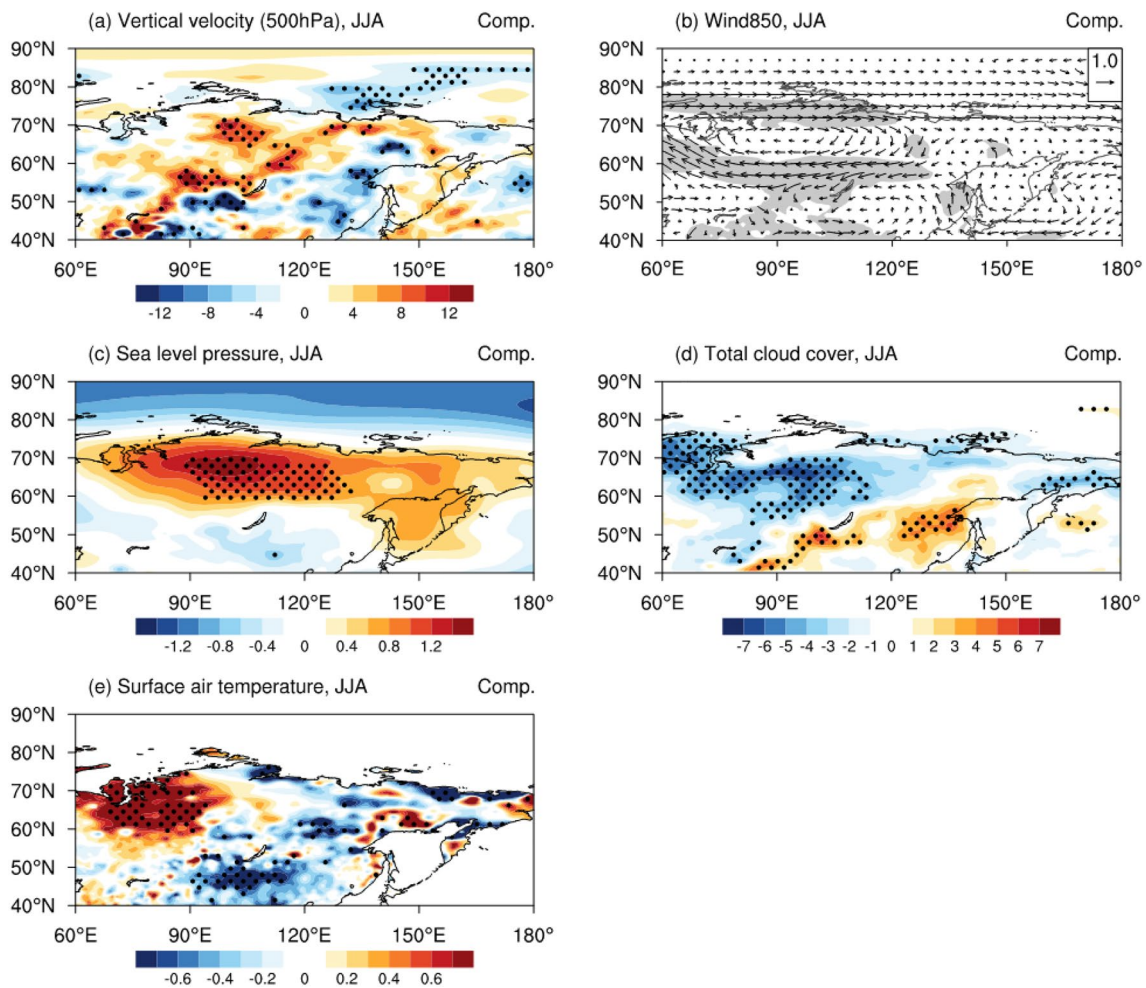
Fig. 3 Differences in summer **a** 500-hPa vertical velocity (units: 10^{-3} Pa s^{-1}), **b** wind fields at 850 hPa (unit: m s^{-1}), **c** sea level pressure (unit: hPa), **d** total cl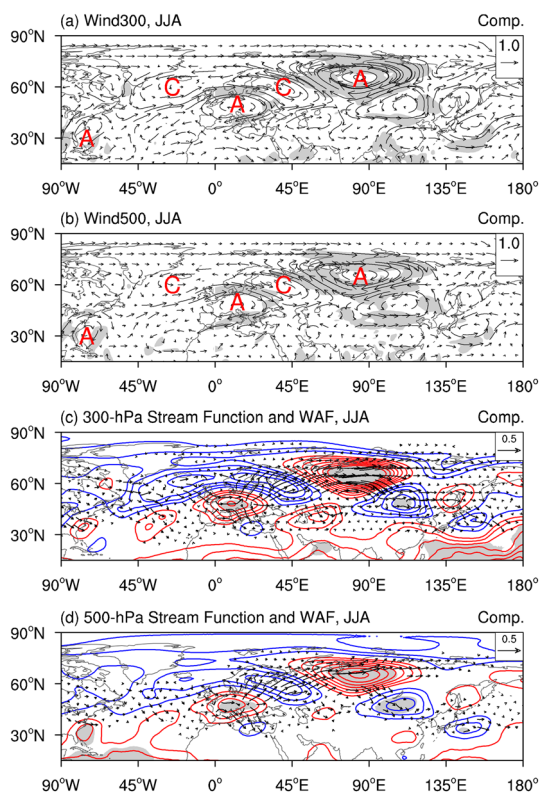oud cover (unit: %) and **e** SAT (unit: °C) between positive (1980–1994 and 2012–2019) and negative (1995–2011) phases based on the ERA-Interim data and CPC Global Temperature data. Areas that exceed the 95% confidence level are dotted
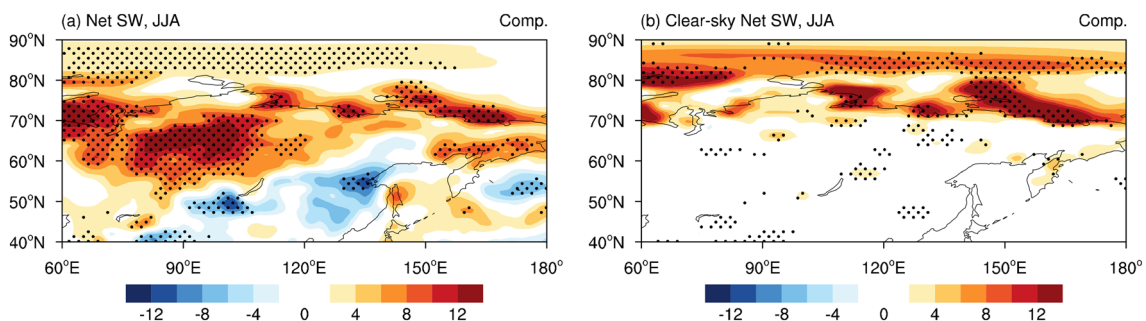
Fig. 4 Differences in summer surface **a** all-sky and **b** clear-sky net shortwave radiation (units: W m^{-2}) between positive (1980–1994 and 2012–2019) and negative (1995–2011) phases based on the ERA-Interim data. Areas that exceed the 95% confidence level are dotted
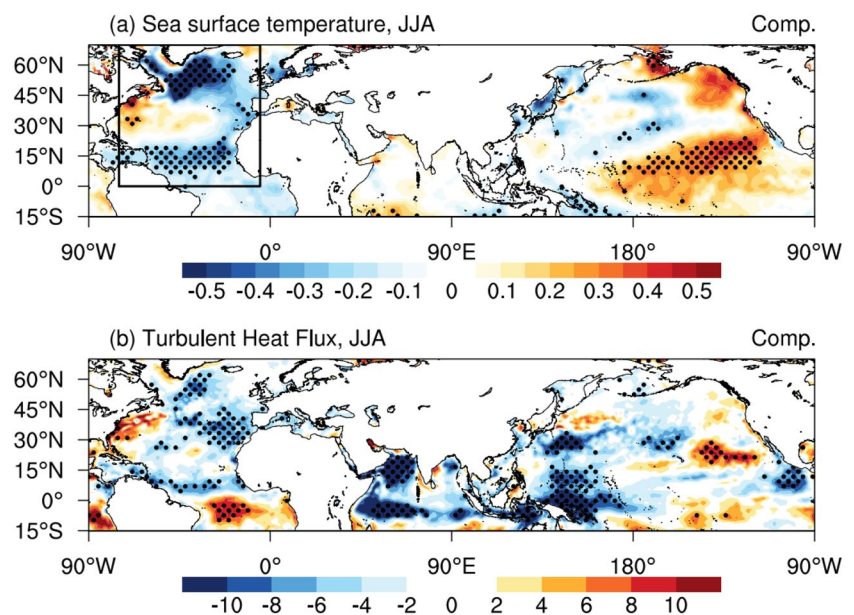
which resembled the decadal changes of tropospheric circulation. Further analysis of WAF suggested that this tropospheric wave train originates from the mid-North Atlantic and propagates eastward (Fig. 8c and d). The centers of convergence and divergence of WAF were consistent with the anticyclone–cyclone pattern. It indicated that the anomalous North Atlantic tripole SST pattern and coupled positive NAO pattern can cause wave activity anomalies and shape

Fig. 5 Differences in summer **a** 300-hPa and **b** 500-hPa wind fields (units: m s^{-1}), **c** 300-hPa and **d** 500-hPa qausi-geostrophic stream function (contours; units: 10^5 m^2 s^{-1}) and WAF (vectors; units: m^2 s^{-2}) between positive (1980–1994 and 2012–2019) and negative (1995–2011) phases based on the ERA-Interim data. Areas with the confidence level exceeding 90% are shaded gray. In a and b the red "A" and "C" letters stand for anticyclonic and cyclonic circulations, respectively. In c and d blue (red) contours represent negative (positive) values
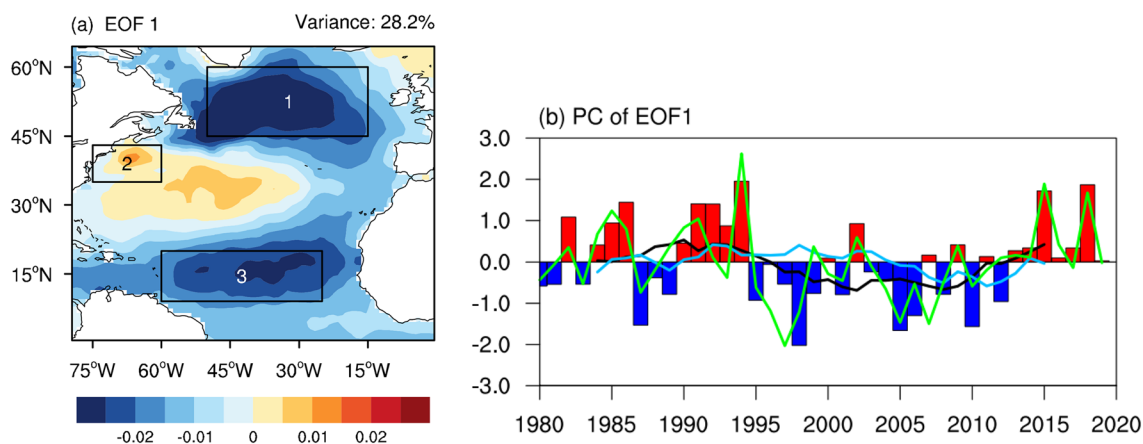
the abovementioned wave train from the North Atlantic to Siberia. Consequently, anticyclonic circulation anomalies led to negative total cloud cover anomalies over western-central Siberia, thereby resulting in higher SAT and more frequent and stronger EHT events there (Fig. 9). This result confirmed the observed decadal linkage between the air–sea interaction in the North Atlantic and increased EHT events in western-central Siberia.

In addition, compared with composite analysis (Fig. 4), the wave train signals were more pronounced in the regression map. It suggested that the eastward wave train probably has more significant impacts on climate in MHLCA on an interannual timescale. Of course, a variety of other factors (such as anthropogenic and natural external forcings, etc.) in the observation might have influences on the above process, and thus can weaken the associated signals on the decadal timescale. More importantly, the length of observational data also limited the analysis of decadal and longer-term changes. Therefore, parallel analysis using a long-term simulation with no variations in external forcing agents was necessary.

3.4 Simulated linkage between North Atlantic climate and EHT

In the long-term CESM simulation, the meridional tripole SST pattern was also the first leading mode of the North Atlantic (Fig. 10a). In its positive phase, positive SST anomalies were evident in the mid-latitude North Atlantic, which were surrounded by negative SST anomalies. Two centers of the negative SST anomalies were located in the Labrador Sea and subtropical North Atlantic, respectively. This simulated tripole SST pattern resembled the observed one.

Fig. 6 Differences in summer **a** observed SST (unit: °C) and **b** turbulent heat fluxes from ERA-Interim data (unit: W m^{-2}) between positive (1980–1994 and 2012–2019) and negative (1995–2011) phases. Areas that exceed the 95% confidence level are dotted. In b the positive value indicates the upward and negative indicates the downward

Fig. 7 a First leading EOF mode of observed summer North Atlantic SST anomalies and **b** its PC during 1980–2019 (bars) along with the nine-year running mean (black line). In **a** black boxes are used to define the summer NATI, representing the subpolar area (region₁: 45°–60° N, 50°–15° W), mid-latitude North Atlantic area (region₂: 35°–43° N, 75°–60° W) and subtropical area (region₃: 9°–20° N, 60°–25° W), respectively. In **b** the green line denotes the normalized NATI, blue line denotes the nine-year running mean summer NAO index calculated with reference to the definition of Folland et al. (2009)
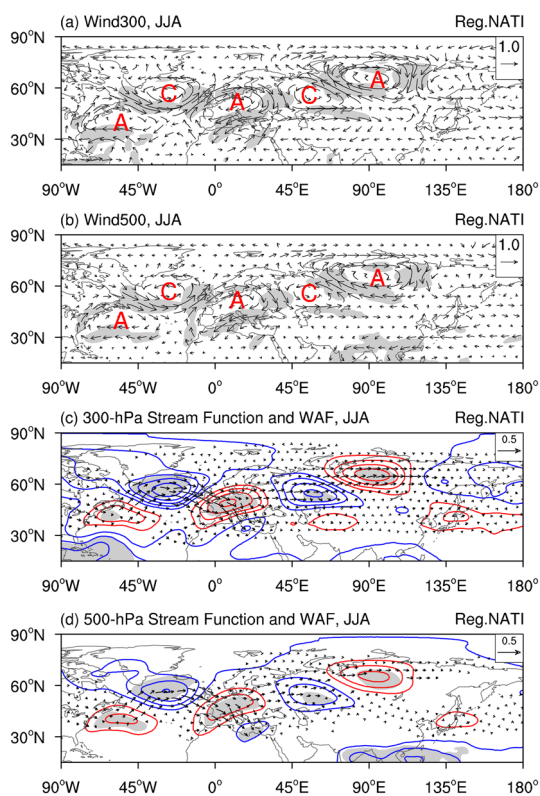

Fig. 8 Regression maps of **a** 300-hPa and **b** 500-hPa wind field anomalies (units: m s^{-1}), **c** 300-hPa and (d) 500-hPa qausi-geostrophic stream function (contours; units: 10^5 m^2 s^{-1}) and WAF (vectors; units: m^2 s^{-2}) anomalies upon the summer NATI. The results are based on the ERA-interim data. Areas that exceed the 95% confidence level are shaded gray. In **a** and **b** the red "A" and "C" letters stand for anticyclonic and cyclonic circulations, respectively. In **c** and **d** blue (red) contours represent negative (positive) values

At the same time, its PC and simulated NATI were consistent and showed significant decadal variabilities (Fig. 10b, c). Particularly, in the second half of this long-term simulation, the 9-year running averages of both the PC and NATI were almost always positive values during model years 46–57 and 94–100, whereas they were almost always negative values during model years 58–93. Thus, focusing on these model years, we examined the corresponding differences in circulation and temperature over the Eurasian continent, and especially the middle and high latitudes of Asia, between different decadal phases of the North Atlantic tripole SST pattern.

As shown in Fig. 11, a similar anomalous circulation pattern can be found in the troposphere over the North Atlantic and Eurasian continental region. Positive NAO-like pattern was evident over the North Atlantic. At the same time, a significant anticyclonic–cyclonic teleconnection wave train propagated from over the island of Newfoundland to Europe, and finally to western-central Siberia, which resembled the results based on the observational data (Figs. 5 , 8). The anomalous tropospheric WAF was also the same, demonstrating eastward propagation characteristics of anomalous circulation signals. Therefore, on the decadal timescale in both the simulation and observation, corresponding to the decadal meridional negative–positive–negative SST pattern in the North Atlantic and positive NAO-like pattern, anomalous anticyclonic circulation was evident in the troposphere over western-central Siberia. As a result, the simulated total cloud cover decreased, ultimately leading to increased SAT in western-central Siberia (Fig. 12). The abovementioned simulated process was almost the same as the observed one, which further confirmed the close linkage between
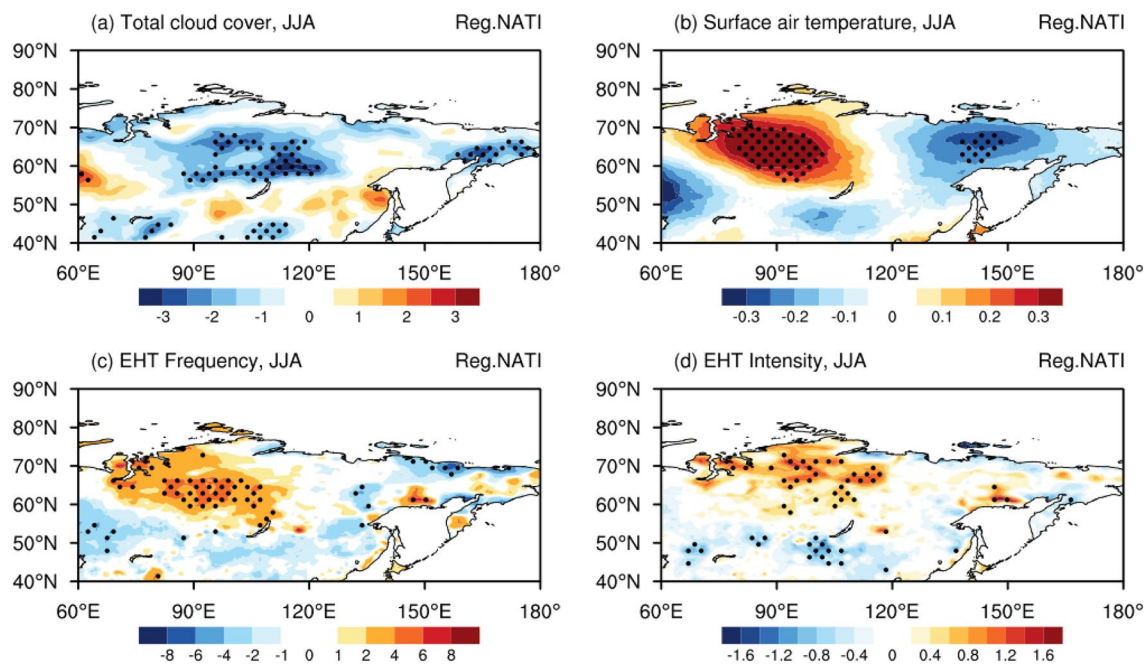
Fig. 9 Regression maps of summer **a** total cloud cover (unit: %), **b** SAT (unit: °C), **c** EHT frequency (unit: days) and **d** EHT intensity (unit: °C) anomalies upon the summer NATI. The results are based on the ERA-interim data and CPC Global Temperature data. Areas that exceed the 95% confidence level are dotted

decadal changes in North Atlantic climate and EHT in western-central Siberia.

In fact, a large number of studies have focused on the air–sea interaction process in the North Atlantic. On the interannual scale, the climate variations over the North Atlantic are related to changes in the NAO (Glowienkahense 1990; Hurrell and VanLoon 1997; Rogers 1997; Frankignoul et al. 2001; Hurrell and Deser 2009). Through large-scale air–sea interaction, the interannual tripole SST pattern in the wintertime North Atlantic Ocean was suggested to be driven by the NAO (e.g., Cayan 1992; Battisti et al. 1995; Marshall et al. 2001a, 2001b; Zhou et al. 2006). However, on decadal and longer timescales, the ocean was thought to significantly contribute to climate variability (Bjerknes 1964; Sutton and Hodson 2003). In the North Atlantic, the oceanic dynamics also played an important role in generating decadal SST anomalies (Eden and Jung 2001; Marshall et al. 2001a, 2001b). In addition, changes in North Atlantic sea ice is also suggested to have an impact on decadal SST variability (Deser et al. 1993). Focusing on the North Atlantic tripole SST pattern in the present study, Häkkinen (2000) indicated the importance of oceanic dynamics in shaping the decadal variation. Gulev et al. (2013) also suggested that, on the decadal timescale, the North Atlantic Ocean can drive the turbulent heat flux and force the atmosphere. Of course, both atmospheric forcing and ocean dynamics may play important roles in the formation of such decadal tripole SST anomaly pattern (Arthun et al. 2021). In this study, to examine the

causes in shaping the wave train and decadal change in EHT in MHLCA, the observed summertime turbulent heat fluxes (sensible plus latent heat fluxes) over the Northern Ocean were diagnosed (Fig. 6b). Similarly, tripole turbulent heat fluxes can be seen over the North Atlantic, corresponding well to the tripole SST anomalies between the positive and negative EHT phases. It indicated that the cooling (warming) North Atlantic SST releases less (more) energy to force the overlying atmosphere at the decadal scale, rather than atmosphere controlled the ocean through anomalous turbulent heat fluxes. From observed changes of the indies, we can also see that the decadal variation of the summer NAO also lags behind that of NATI (Fig. 6b). Thus, on the decadal scale, SST variation may play a more important role in regulating the overlying atmosphere.
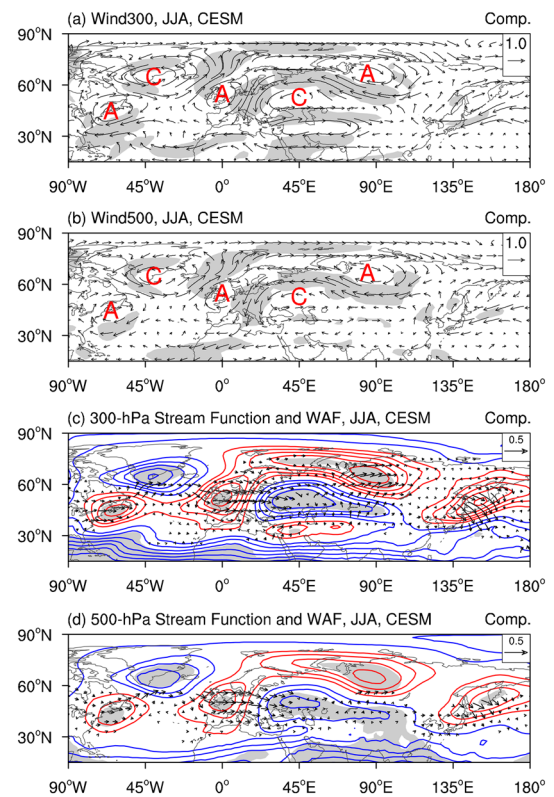
To further identify the driving effects of North Atlantic tripole SST on the wave train and decadal changes in EHT in MHLCA, two simulations using the CAM5 were performed. The configure set "F_2000_CAM5" was selected for them. It meant that the atmospheric composition was constant in the year 2000. The resolution was 2.5° longitude × 1.9° latitude, with 26 vertical hybrid levels. The first simulation was a control run with the model's modern climatological SST and sea ice (hurrell_sst_ifrac.1 × 1.050606.nc, which is the default setting of SST and sea ice cover climatological data used by CAM to simulate present climate). The second simulation was a sensitivity run, an idealised SST was constructed by imposing the observed differences in
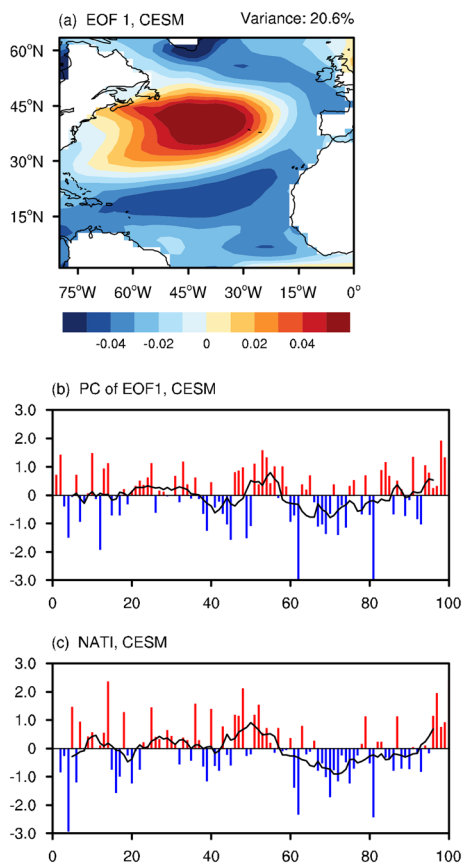
Fig. 10 **a** First leading EOF mode of CESM simulated summer North Atlantic SST anomalies and **b** its PC (color bars) and corresponding 9-year running mean (black line). **c** Simulated summer NATI and (color bars) and its 9-year running mean (black line)

Fig. 11 Differences in CESM simulated summer **a** 300-hPa and **b** 500-hPa wind fields (units: m s^{-1}), **c** 300-hPa and **d** 500-hPa qausi-geostrophic stream function (contours; units: 10^5 m^2 s^{-1}) and WAF (vectors; units: m^2 s^{-2}) anomalies between positive and negative NATI phases. Areas that exceed the 90% confidence level are shaded gray. In a and b the red "A" and "C" letters stand for anticyclonic and cyclonic circulations, respectively. In c and d blue (red) contours represent negative (positive) values

summer SST between positive and negative phases in the North Atlantic (black box in Figs. 6a 0°~70° N in the North Atlantic Ocean) on the control run's monthly climatological SSTs from June to August. Both simulations were consecutively integrated for 50 years. The results analyzed represent averages for the final 40 years, allowing 10 years for the model to a relative equilibrium state. The only differences between these two simulations were the decadal tripole SST anomalies in the North Atlantic. Therefore, the comparison between them highlighted the influences of anomalous tripole SSTs on the overlying atmosphere and change in EHT in MHLCA.

As shown in Fig. 13, the tripole-like SAT anomalies were evident in the North Atlantic, which well responded to the SST boundary forcing. At the same time, significant surface warming can be found in western-central Siberia. Similar with processes in the observations and coupled model, an anomalous anticyclonic–cyclonic teleconnection wave train was simulated from the North Atlantic to Siberia. Thus, the local anticyclonic conditions led to the reduced total cloud cover and thereby the surface warming in western-central

Siberia (figure not shown). It indicated that the tripole SST anomalies in the North Atlantic can cause lead to decadal change in EHT in MHLCA by causing anomalous atmospheric meridional temperature gradient over the North Atlantic and related large-scale circulation anomalies over Eurasia. In addition, we can find that the cyclone and anticyclone centers of the wave train simulated by CAM5 were weaker and slightly displaced from the observed and CESM simulated positions. It implied that the air–sea coupling process may also play an important role in strengthening the excitation and downstream propagation of wave trains.

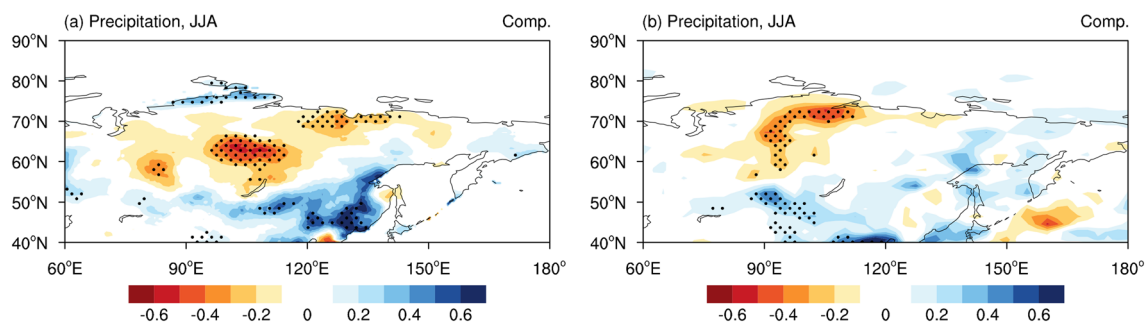## 3.5 Potential precipitation-related feedback

In the past two decades, more compound hot and dry extremes have been reported worldwide (e.g., AghaKouchak et al. 2014; Miralles et al. 2014; Wu et al. 2021). Enhanced land–atmosphere coupling, associated with persistent soil moisture deficits, appeared to intensify surface warming and anticyclonic circulation anomalies, and thereby leading to
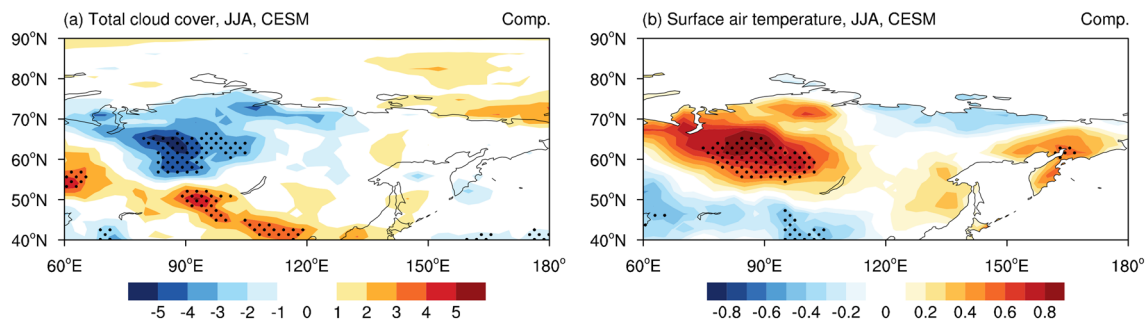
Fig. 12 Differences in CESM simulated summer **a** total cloud cover (unit: %) and **b** SAT (unit: °C) between positive and negative NATI phases. Areas that exceed the 95% confidence level are dotted
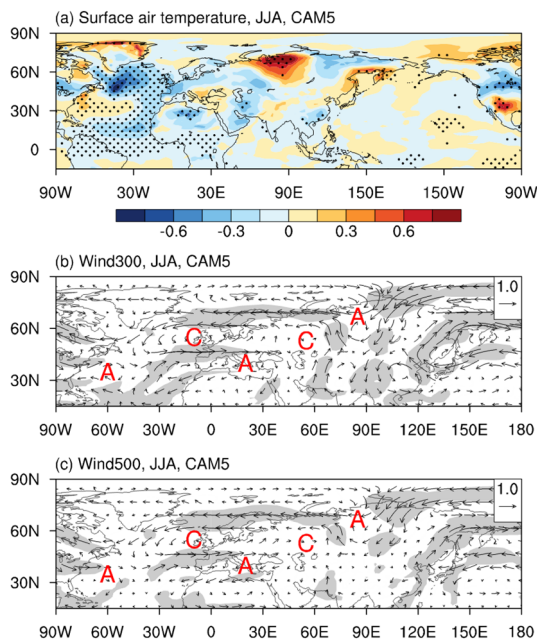
Fig. 13 Differences in CAM5 simulated summer **a** SAT (unit: °C), **b** 300-hPa and **c** 500-hPa wind fields (units: m s^{-1}) between the sensitivity run and control run. Areas that exceed the 95% confidence level are dotted or shaded gray. In b and c the red "A" and "C" letters stand for anticyclonic and cyclonic circulations, respectively

stronger EHT events (Zhang et al. 2020b). In this positive feedback process, a reduction in precipitation was also one of the important processes (Miralles et al. 2019).

Focusing on the present study, in both the observation and simulation, decreased precipitation was evident over the central Siberian region, whereas increased precipitation was apparent over the south of Lake Baikal (Fig. 14). In the Siberia, the decreased precipitation was likely caused by the decreased SST in the tropical and high-latitude Atlantic (Sun et al. 2015; Nicolì et al. 2020). At the same time, this precipitation anomaly pattern was partially consistent with anomalous EHT events, suggesting that precipitation-related feedback was possibly involved in the decadal variability of EHT events in MHLCA.

4 Conclusion and discussion

In this study, the observed spatiotemporal characteristics of EHT events in MHLCA (the mid and high latitudes of continental Asia) were investigated. After removing the linear trend, significant decadal variation of EHT events could be found in the observation. During the periods 1980–1994 and 2012–2019, EHT events were more frequent and stronger in western-central Siberia than normal,

Fig. 14 Differences in **a** observed (CRU data set) and **b** CESM simulated summer precipitation (units: mm d^{-1}) between positive and negative phases. Areas that exceed the 95% confidence level are dotted

whereas they were less frequent and weaker in the wide area south of Lake Baikal. The pattern of anomalous EHT events was found to show a meridional mode, and during the period 1995–2011 this EHT event pattern reversed.

Further analysis indicated that the decadal North Atlantic tripole SST anomaly pattern and associated sea–air interaction played important roles in shaping the above-mentioned decadal variability of EHT events in MHLCA. During a positive NATI phase (i.e., negative–positive–negative SST anomaly phase), stronger eastward propagation of WAF (wave activity flux) can cause a significant anticyclonic–cyclonic teleconnection wave train in the troposphere over the mid and high latitudes of the Eurasian continent. Anomalous anticyclonic circulation was evident over western-central Siberia, which led to an anomalous high-pressure center and reduced total cloud cover; and because of stronger solar radiation heating, EHT events became more frequent and stronger in this region. In addition, anomalous anticyclonic circulation also caused an anomalous cyclonic condition over the wide area to the south of Lake Baikal, which reduced the frequency and weakened the severity of EHT events there. Results based on a long-term CESM simulation confirmed the important role of North Atlantic air–sea interaction in abovementioned processes. Further analysis based on the observed turbulent heat fluxes and CAM5 simulations suggested that, at the decadal scale, the tripole SST was likely to play a more important driving role.

It was noted that there were also significant positive SST anomalies in the subtropical Pacific between positive and negative EHT phases (Fig. 6a). Analysis based on observations cannot infer whether the positive SST anomalies contribute to the warming in western-central Siberia. It was interesting that CAM simulations produce similar warming in the eastern subtropical Pacific (Fig. 13a). It implied that the North Atlantic tripole SST anomalies might be important factor leading to positive SST anomalies in the subtropical Pacific through atmospheric bridges, which needs further investigation.

Recently, Hong et al. (2022) also investigated variations of EHT events in MHLCA, with a particular focus on interannual-scale physical processes. The Polar–Eurasian teleconnection pattern, NAO and Pacific–Japan/East Asia–Pacific pattern were all suggested to be the atmospheric factors in regulating the EHT events in MHLCA on the interannual scale. The related local physical processes were consistent with the present study. At the same time, they further pointed out the contribution of Atlantic multidecadal oscillation (AMO) and global warming to the long-term trend of EHT events in the region. In this study, however, we focused more on the impacts of decadal variability on extreme events in MHLCA, and indicated the roles of the decadal North Atlantic tripole SST anomaly and its coupled atmospheric circulation.

In this study, the analyses based on observations were detrended, and the external forcing factors such as greenhouse gases in the long-term simulations were kept constant. This means that the study highlighted the impact of decadal-scale internal variability in the climate system on MHLCA extreme weather events. Numerous studies have projected EHT events/heatwaves to become more frequent and stronger in the future (e.g., Zhou et al. 2016; Bador et al. 2017; Chen and Dong 2021; Rasmijn et al. 2018; Yin et al. 2020). Based on an early model result, Meehl and Tebaldi (2004) suggested that the European and North American heat-wave-related atmospheric circulation pattern will be intensified by ongoing increases in greenhouse gas concentrations, which in turn will lead to more severe heat waves.

In the MHLCA region, warming is more pronounced due to the Arctic amplification effect. However, it remains unclear whether the coupling process of the North Atlantic at the decadal scale will change under a more intense warming background in the future, and whether the large-scale circulation anomalies generated from the North Atlantic coupled processes will be affected by global warming. Firstly, the increase in global average temperature can significantly contribute to the enhancement of EHT events (e.g., Dong et al. 2017). Against the background of future warming, it is necessary to further investigate whether the circulation system related to decadal-scale internal variability of the North Atlantic will strengthen and further increase the intensity and frequency of EHT using the multimodel results from the latest two phases (5 and 6) of CMIP.

in the Sect. 2 and the simulation results section, respectively. They are also available from the corresponding author on reasonable request.

Declarations

Conflicts of interest The authors declare no conflicts of interest.

Open Access This article is licensed under a Creative Commons Attribution 4.0 International License, which permits use, sharing, adaptation, distribution and reproduction in any medium or format, as long as you give appropriate credit to the original author(s) and the source, provide a link to the Creative Commons licence, and indicate if changes were made. The images or other third party material in this article are included in the article's Creative Commons licence, unless indicated otherwise in a credit line to the material. If material is not included in the article's Creative Commons licence and your intended use is not permitted by statutory regulation or exceeds the permitted use, you will need to obtain permission directly from the copyright holder. To view a copy of this licence, visit http://creativecommons.org/licenses/by/4.0/.

References

Adams RE, Lee CMC, Smith ET, Sheridan SC (2021) The relationship between atmospheric circulation patterns and extreme temperature events in North America. Int J Climatol 41:92–103

AghaKouchak A, Cheng LY, Mazdiyasni O, Farahmand A (2014) Global warming and changes in risk of concurrent climate extremes: insights from the 2014 California drought. Geophys Res Lett 41:8847–8852

Arblaster JM, Alexander LV (2012) The impact of the El Nino-Southern Oscillation on maximum temperature extremes. Geophys Res Lett 39:L20702

Arthun M, Wills RCJ, Johnson HL, Chafik L, Langehaug HR (2021) Mechanisms of decadal North Atlantic climate variability and implications for the recent cold anomaly. J Clim 34:3421–3439

Bador M, Terray L, Boe J, Somot S, Alias A, Gibelin AL, Dubuisson B (2017) Future summer mega-heatwave and record-breaking temperatures in a warmer France climate. Environ Res Lett 12:074025

Barriopedro D, Fischer EM, Luterbacher J, Trigo R, Garcia-Herrera R (2011) The hot summer of 2010: redrawing the temperature record map of Europe. Science 332:220–224

Battisti DS, Bhatt US, Alexander MA (1995) A modeling study of the interannual variability in the wintertime North Atlantic Ocean. J Clim 8:3067–3083

Bjerknes J (1964) Atlantic air–sea interaction. Adv Geophys 10:1–82

Bonsal BR, Zhang X, Vincent LA, Hogg WD (2001) Characteristics of daily and extreme temperatures over Canada. J Clim 14:1959–1976

Bouchama A (2004) The 2003 European heat wave. Intens Care Med 30:1–3

Cayan DR (1992) Latent and sensible heat flux anomalies over the Northern oceans: driving the sea surface temperature. J Phys Oceanogr 22:859–881

Chen W, Dong BW (2019) Anthropogenic impacts on recent decadal change in temperature extremes over China: relative roles of greenhouse gases and anthropogenic aerosols. Clim Dynam 52:3643–3660

Chen W, Dong BW (2021) Projected near-term changes in temperature extremes over China in the mid-twenty-first century and underlying physical processes. Clim Dynam 56:1879–1894

Chen HP, Sun JQ (2015) Changes in climate extreme events in China associated with warming. Int J Climatol 35:2735–2751

Cheng LJ, Abraham J, Hausfather Z, Trenberth KE (2019) How fast are the oceans warming? Science 363:128–129

Christidis N, Stott PA (2016) Attribution analyses of temperature extremes using a set of 16 indices. Weather and Climate Extremes 14:24–35

Christidis N, Stott PA, Brown SJ (2011) The role of human activity in the recent warming of extremely warm daytime temperatures. J Clim 24:1922–1930

China Meteorological Administration (2014) China Climate Bulletin 2013

Coumou D, Rahmstorf S (2012) A decade of weather extremes. Nat Clim Change 2:491–496

Coumou D, Robinson A, Rahmstorf S (2013) Global increase in record-breaking monthly-mean temperatures. Clim Change 118:771–782

Cowan T, Hegerl GC, Colfescu I, Bollasina M, Purich A, Boschat G (2017) Factors contributing to record-breaking heat waves over the Great Plains during the 1930s Dust Bowl. J Clim 30:2437–2461

Dee DP (2011) The ERA-Interim reanalysis: configuration and performance of the data assimilation system. Q J Roy Meteor Soc 137:553–597

Deng KQ, Yang S, Ting MF, Zhao P, Wang ZY (2019) Dominant Modes of China Summer Heat waves driven by Global Sea Surface Temperature and Atmospheric Internal Variability. J Clim 32:3761–3775

Deng KQ, Yang S, Gu DJ, Lin AL, Li CH (2020) Record-breaking heat wave in southern China and delayed onset of South China Sea summer monsoon driven by the Pacific subtropical high. Clim Dynam 54:3751–3764

Deser C, Blackmon ML (1993) Surface climate variations over the North-Atlantic Ocean during Winter-1900–1989. J Clim 6:1743–1753

Diao YF, Li T, Hsu PC (2018) Influence of the boreal summer intraseasonal oscillation on extreme temperature events in the Northern Hemisphere. J Meteorol Res 32:534–547

Donat M, Alexander L, Yang H, Durre I, Vose R, Caesar J (2013) Global land-based datasets for monitoring climatic extremes. Bull Am Meteorol Soc 94:997–1006

Dong BW, Sutton RT, Chen W, Liu XD, Lu RY, Sun Y (2016) Abrupt summer warming and changes in temperature extremes over Northeast Asia since the mid-1990s: drivers and physical processes. Adv Atmos Sci 33:1005–1023

Dong BW, Sutton RT, Shaffrey L (2017) Understanding the rapid summer warming and changes in temperature extremes since the mid-1990s over Western Europe. Clim Dynam 48:1537–1554

Eden C, Jung T (2001) North Atlantic interdecadal variability: Oceanic response to the North Atlantic oscillation (1865–1997). J Clim 14:676–691

Fischer EM, Knutti R (2015) Anthropogenic contribution to global occurrence of heavy-precipitation and high-temperature extremes. Nat Clim Change 5:560–564

Fischer EM, Seneviratne SL, Vidale PL, Luthi D, Schar C (2007) Soil moisture–atmosphere interactions during the 2003 european summer heat wave. J Clim 20:5081–5099

Folland CK, Knight J, Linderholm HW, Fereday D, Ineson S, Hurrell JW (2009) The summer North Atlantic oscillation: past, present, and future. J Clim 22:1082–1103

Founda D, Giannakopoulos C (2009) The exceptionally hot summer of 2007 in Athens, Greece— A typical summer in the future climate? Global Planet Change 67:227–236

Frankignoul C, de Coetlogon G, Joyce TM, Dong SF (2001) Gulf stream variability and ocean-atmosphere interactions. J Phys Oceanogr 31:3516–3529

Glowienkahense R (1990) The North-Atlantic Oscillation in the Atlantic-European Slp. Tellus Series - Dyn Meteorol and Oceanogr 42:497–507

Griffiths GM, Coauthors (2005) Change in mean temperature as a predictor of extreme temperature change in the Asia-Pacific region. Int J Climatol 25:1301–1330

Gu SH, Huang CR, Bai L, Chu C, Liu QY (2016) Heat-related illness in China, summer of 2013. Int J Biometeorol 60:131–137

Gulev SK, Latif M, Keenlyside N, Park W, Koltermann KP (2013) North Atlantic Ocean control on surface heat flux on multidecadal timescales. Nature 499:464–468

Häkkinen S (2000) Decadal air-sea interaction in the North Atlantic based on observations and modeling results. J Clim 13:1195–1219

Harris I, Osborn TJ, Jones P, Lister D (2020) Version 4 of the CRU TS monthly high-resolution gridded multivariate climate dataset. Sci Data 7(1):109

Hong HX, Sun JQ, Wang HJ (2022) Variations in summer extreme high-temperature events over northern Asia and the possible mechanisms. J Clim 35:335–357

Horton DE, Johnson NC, Singh D, Swain DL, Rajaratnam B, Diffenbaugh NS (2015) Contribution of changes in atmospheric circulation patterns to extreme temperature trends. Nature 522:465–469

Hu KM, Huang G, Wu RG (2013) A strengthened influence of ENSO on August high temperature extremes over the Southern Yangtze River Valley since the late 1980s. J Clim 26:2205–2221

Hurrell JW, Deser C (2009) North Atlantic climate variability: the role of the North Atlantic Oscillation. J Mar Syst 78:28–41

Hurrell JW, VanLoon H (1997) Decadal variations in climate associated with the north Atlantic oscillation. Clim Change 36:301–326

IPCC (2013) Climate Change 2013 The Physical Science Basis. In: Stocker TF, Qin D, Plattner G-K(eds) Contribution of Working Group I to the Fifth Assessment Report of the Intergovernmental Panel on Climate Change. Cambridge University Press, United Kingdom

IPCC (2021) Climate change 2021 the physical science basis. In:Masson-Delmotte V, Zhai P, Pirani A(eds)Contribution of Working Group I to the Sixth Assessment Report of the Intergovernmental Panel on Climate Change. Cambridge University Press, United Kingdom

Kim YH, Min SK, Zhang XB, Zwiers F, Alexander LV, Donat MG, Tung YS (2016) Attribution of extreme temperature changes during 1951–2010. Clim Dynam 46:1769–1782

Kushnir Y (1994) Interdecadal variations in North-Atlantic Sea-Surface temperature and associated atmospheric conditions. J Clim 7:141–157

Lau N-C, Nath MJ (2012) A model study of heat waves over North America: meteorological aspects and projections for the twenty-first century. J Clim 25:4761–4784

Lau N-C, Nath MJ (2014) Model simulation and projection of European heat waves in present-day and future climates. J Clim 27:3713–3730

Li Y, Ding YH, Liu YX (2021) Mechanisms for regional compound hot extremes in the mid-lower reaches of the Yangtze River. Int J Climatol 41:1292–1304

Loikith PC, Broccoli AJ (2012) Characteristics of observed Atmospheric circulation patterns Associated with temperature extremes over North America. J Clim 25:7266–7281

Lu R, Zhu ZW, Li T, Zhang HY (2020) Interannual and interdecadal variabilities of spring rainfall over Northeast China and their associated sea surface temperature anomaly forcings. J Clim 33:1423–1435

Luo M, Lau NC (2017) Heat waves in Southern China: synoptic behavior, long-term change, and urbanization effects. J Clim 30:703–720

Marshall J, Johnson H, Goodman J (2001a) A study of the interaction of the North Atlantic oscillation with ocean circulation. J Clim 14:1399–1421

Marshall J, Kushner Y, Battisti D, Chang P, Czaja A, Dickson R, Hurrell J, McCartney M, Saravanan R, Visbeck M (2001b) North Atlantic climate variability: phenomena, impacts and mechanisms. Int J Climatol 21(15):1863–1898

Meehl GA, Tebaldi C (2004) More intense, more frequent, and longer lasting heat waves in the 21st century. Science 305:994–997

Meehl GA, Arblaster JM, Tebaldi C (2007) Contributions of natural and anthropogenic forcing to changes in temperature extremes over the United States. Geophys Res Lett 34:L19709

Miralles DG, Teuling AJ, van Heerwaarden CC, de Arellano JVG (2014) Mega-heatwave temperatures due to combined soil desiccation and atmospheric heat accumulation. Nat Geosci 7:345–349

Miralles DG, Gentine P, Seneviratne SI, Teuling AJ (2019) Land-atmospheric feedbacks during droughts and heatwaves: state of the science and current challenges. Ann NY Acad Sci 1436:19–35

Morak S, Hegerl GC, Christidis N (2013) Detectable changes in the frequency of temperature extremes. J Clim 26:1561–1574

Nicolì D, Bellucci A, Iovino D, Ruggieri P, Gualdi S (2020) The impact of the AMV on eurasian summer hydrological cycle. Sci Rep 10:14444

Rahmstorf S, Coumou D (2011) Increase of extreme events in a warming world. Proc Natl Acad Sci USA 108:17905–17909

Rasmijn LM, van der Schrier G, Bintanja R, Barkmeijer J, Sterl A, Hazeleger W (2018) Future equivalent of 2010 russian heatwave intensified by weakening soil moisture constraints. Nat Clim Change 8:381–386

Rayner NA, Coauthors (2003) Global analyses of sea surface temperature, sea ice, and night marine air temperature since the late nineteenth century. J Geophys Res-Atmos 108:4407

Rogers JC (1997) North Atlantic storm track variability and its association to the north Atlantic oscillation and climate variability of northern Europe. J Clim 10:1635–1647

Schär C, Vidale PL, Luthi D, Frei C, Häberli C, Liniger MA, Appenzeller C (2004) The role of increasing temperature variability in European summer heatwaves. Nature 427:332–336

Schlesinger ME, Ramankutty N (1994) An oscillation in the global climate system of period 65–70 years. Nature 367:723–726

Screen JA, Simmonds I (2010) The central role of diminishing sea ice in recent Arctic temperature amplification. Nature 464:1334–1337

Seong MG, Min SK, Kim YH, Zhang XB, Sun Y (2021) Anthropogenic greenhouse gas and aerosol contributions to extreme temperature changes during 1951–2015. J Clim 34:857–870

Shiogama H, Watanabe M, Imada Y, Mori M, Kamae Y, Ishii M, Kimoto M (2014) Attribution of the June–July 2013 Heat Wave in the Southwestern United States. Sola 10:122–126

Stefanon M, Drobinski P, D'Andrea F, Lebeaupin-Brossier C, Bastin S (2014) Soil moisture–temperature feedbacks at meso-scale during summer heat waves over Western Europe. Clim Dynam 42:1309–1324

Sun C, Li JP, Zhao S (2015) Remote influence of Atlantic multidecadal variability on siberian warm season precipitation. Sci Rep 5:16853

Sun Y, Song LC, Yin H, Zhang XB, Stott P, Zhou BT, Hu T (2016) Human influence on the 2015 extreme high temperature events in Western China. Bull Am Meteorol Soc 97:S102–S106

Sutton RT, Hodson DLR (2003) Influence of the ocean on North Atlantic climate variability 1871–1999. J Clim 16:3296–3313

Tomczyk AM, Bednorz E (2016) Heat waves in Central Europe and their circulation conditions. Int J Climatol 36:770–782

Wang WW, Zhou W, Wang X, Fong SK, Leong KC (2013) Summer high temperature extremes in Southeast China associated with the east asian jet stream and circumglobal teleconnection. J Geophys Res-Atmos 118:8306–8319

Wang WW, Zhou W, Chen DL (2014) Summer High temperature extremes in Southeast China: bonding with the El Nino-Southern Oscillation and East Asian summer monsoon coupled system. J Clim 27:4122–4138

Wu XY, Hao ZC, Hao FH, Zhang X, Singh VP, Sun C (2021) Influence of large-scale circulation patterns on compound dry and hot events in China. J Geophys Res-Atmos 126:e2020JD033918

Xie SP et al (2015) Towards predictive understanding of regional climate change. Nat Clim Change 5:921–930

Xu YY, Ramanathan V, Victor DG (2018) Global warming will happen faster than we think. Nature 564:30–32

Xu PQ, Wang L, Chen W (2019a) The British-Baikal Corridor: a Teleconnection pattern along the summertime polar front jet over Eurasia. J Clim 32:877–896

Xu K, Lu R, Mao J, Chen R (2019b) Circulation anomalies in the mid–high latitudes responsible for the extremely hot summer of 2018 over northeast Asia. Atmos Ocean Sci Lett 12:231–237

Xu PQ, Wang L, Liu YY, Chen W, Huang P (2020) The record-breaking heat wave of June 2019 in Central Europe. Atmos Sci Lett 21(4):e964

Yang XY, Zeng G, Zhang GW, Li JW, Li ZX, Hao ZX (2021) Interdecadal variations of different types of summer heatwaves in Northeast China associated with AMO and PDO. J Clim. https://doi.org/10.1175/JCLI-D-20-0939.1

Yin SY, Coauthors (2020) Mid-summer surface air temperature and its internal variability over China at 1.5 degrees C and 2 degrees C global warming. Adv Clim Change Res 11:185–197

Yin H, Sun Y, Wan H, Zhang XB, Lu CH (2017) Detection of anthropogenic influence on the intensity of extreme temperatures in China. Int J Climatol 37:1229–1237

Zhang P, Coauthors (2020b) Abrupt shift to hotter and drier climate over inner east Asia beyond the tipping point. Science 370:1095–1099

Zhang ZQ, Sun XG, Yang XQ (2018) Understanding the interdecadal variability of east asian summer monsoon precipitation: joint influence of three oceanic signals. J Clim 31:5485–5506

Zhang GW, Zeng G, Li C, Yang XY (2020a) Impact of PDO and AMO on interdecadal variability in extreme high temperatures in North China over the most recent 40-year period. Clim Dynam 54:3003–3020

Zhou TJ, Yu RC, Gao YQ, Drange H (2006) Ocean-atmosphere coupled model simulation of North Atlantic interannual variability I: local air-sea interaction. Acta Meteor Sinica 64:1–17 (**in Chinese with English abstract**)

Zhou BT, Wen QH, Xu Y, Song LC, Zhang XB (2014) Projected changes in temperature and precipitation extremes in China by the CMIP5 multimodel ensembles. J Clim 27:6591–6611

Zhou BT, Xu Y, Wu J, Dong SY, Shi Y (2016) Changes in temperature and precipitation extreme indices over China: analysis of a high-resolution grid dataset. Int J Climatol 36:1051–1066

Zhu BY, Sun B, Li H, Wang HJ (2020) Interdecadal variations in Extreme High-Temperature events over Southern China in the early 2000s and the influence of the Pacific Decadal Oscillation. Atmosphere-Basel 11:829

Zwiers FW, Zhang XB, Feng Y (2011) Anthropogenic influence on long return period daily temperature extremes at regional scales. J Clim 24:881–892